

Pressure-induced ferroelectric to antiferroelectric phase transition in $\text{Pb}_{0.99}(\text{Zr}_{0.95}\text{Ti}_{0.05})_{0.98}\text{Nb}_{0.02}\text{O}_3$

Maxim Avdeev, James D. Jorgensen, and Simine Short
 Argonne National Laboratory, Argonne, Illinois 60636, USA

George A. Samara, Eugene L. Venturini, Pin Yang, and Bruno Morosin
 Sandia National Laboratories, Albuquerque, New Mexico 87185, USA

(Received 7 February 2005; revised manuscript received 23 September 2005; published 9 February 2006; corrected 29 March 2006)

Zr-rich, Nb-doped lead zirconate titanate ceramic and powder samples with composition near $\text{Pb}_{0.99}(\text{Zr}_{0.95}\text{Ti}_{0.05})_{0.98}\text{Nb}_{0.02}\text{O}_3$ [PZT95/5(2Nb)] have been studied in the range of hydrostatic pressure 0–6.2 kbar and temperature 12–295 K by time-of-flight neutron powder diffraction and dielectric measurements. The combination of the two techniques has led to further insights into the properties and pressure-induced ferroelectric rhombohedral $R3c$ ($F_{R(\text{LT})}$) to antiferroelectric orthorhombic $Pbam$ (A_O) phase transition in this material, and the diffraction results have provided a detailed view of the ionic displacements induced by changes in pressure and temperature as well as the displacements accompanying the transition. At 295 K the diffraction results revealed a sharp transition at 2.1 kbar; at 200 K this transition occurs at 1.1 kbar. The transformation is incomplete: after the initial sharp drop in the $F_{R(\text{LT})}$ content at the transition, 20 wt % of the sample remains in the low-pressure $F_{R(\text{LT})}$ phase. Above the transition, the fraction of $F_{R(\text{LT})}$, which exists as a minority phase in the high-pressure A_O phase, continues to decrease, but even at our highest pressure of 6.2 kbar, ~ 8 wt % of the sample remains in the $F_{R(\text{LT})}$ phase. The volume contraction at the $F_{R(\text{LT})}$ -to- A_O transition unexpectedly results in the retained minority $F_{R(\text{LT})}$ being anisotropically “clamped,” with its a axis slightly expanded and c axis contracted at the transition. On pressure release to 1 bar at 295 K, only 26% of the $F_{R(\text{LT})}$ phase is recovered, and this remains in the clamped state because of the surrounding majority A_O phase. Heating the sample above 350 K at 1 bar followed by cooling to room temperature results in full recovery of the $F_{R(\text{LT})}$ phase. The spontaneous polarization (P_S) of the $F_{R(\text{LT})}$ phase and its pressure and temperature dependences were determined from the ionic displacements. At 295 K, $P_S = 38 \mu\text{C}/\text{cm}^2$ —a value greater than the 31–32 $\mu\text{C}/\text{cm}^2$ commonly observed on ceramic PZT95/5(2Nb) samples. The difference is undoubtedly related to residual porosity in ceramic samples as well as the inability of the poling electric field to align all the polar domains. P_S increases monotonically with decreasing temperature, reaching a value of $\sim 44 \mu\text{C}/\text{cm}^2$ at 12 K.

DOI: [10.1103/PhysRevB.73.064105](https://doi.org/10.1103/PhysRevB.73.064105)

PACS number(s): 61.50.Ks, 61.12.Ld, 77.84.Dy, 64.70.Kb

I. INTRODUCTION AND MOTIVATION

The perovskites PbZrO_3 and PbTiO_3 form a continuous series of solid solutions of the form $\text{PbZr}_{1-x}\text{Ti}_x\text{O}_3$ over the whole composition range. These solid solutions, commonly called PZTs, are rich in the variety of ferroelectric and non-ferroelectric transitions that can be induced in them by variations in composition, temperature (T), electric field, or pressure (P ; stress). They also exhibit large spontaneous polarizations and piezoelectric coefficients. These factors along with their availability in high-quality ceramic form are responsible for their widespread technological usage in applications based on piezoelectric and ferroelectric properties.^{1,2}

For the Zr-rich part of the temperature-composition phase diagram for the PZT system,¹ the high- T phase is paraelectric (PE) and has the ideal cubic perovskite ($Pm\bar{3}m$) structure. On cooling, this phase transforms either to a rhombohedral ferroelectric (FE) phase or to an orthorhombic ($Pbam$) antiferroelectric (AFE), A_O , phase. The rhombohedral ferroelectric region is actually divided into two phases: a high-temperature phase of symmetry $R3m$ ($F_{R(\text{HT})}$) and a low-temperature phase of symmetry $R3c$ ($F_{R(\text{LT})}$), which has a unit cell double that of the $R3m$ phase. All of these phase transitions are known to be associated with lattice dynamical instabilities, or soft phonon modes. Small ionic displacements accompany such transitions, and hence they are often called displacive transitions.

ments accompany such transitions, and hence they are often called displacive transitions.

A particularly interesting member of the PZT family is the composition $\text{PbZr}_{0.95}\text{Ti}_{0.05}\text{O}_3$, or PZT95/5. It has become customary to add a small amount of Nb to this composition to stabilize the $F_{R(\text{LT})}$ phase at ambient conditions and to reduce dielectric losses. On cooling at 1 bar it transforms from the PE phase to the high- T $F_{R(\text{HT})}$ phase and then, near room T , to the low- T $F_{R(\text{LT})}$ phase. Application of modest hydrostatic P induces a transition to the A_O phase. Fritz and Keck³ investigated this transition and determined the T - P phase diagram for PZT95/5 with 2 at. % Nb. Studies by Noheda *et al.*,⁴ Garcia *et al.*,⁵ and Kojima *et al.*⁶ as well as Yang *et al.*⁷ in this Zr-rich region of the phase diagram at various Nb concentrations show that the positions of the $F_{R(\text{HT})}$ - $F_{R(\text{LT})}$ and $F_{R(\text{LT})}$ - A_O transitions and the triple point of the pure PZT diagram shift substantially, as if ~ 1 at. % Nb is equivalent to a Zr enrichment of $\sim 1.3\%$. Kojima *et al.*⁶ extended their measurements to temperatures below room T . (Note that many studies employ 1 wt % Nb_2O_5 which is ~ 2.6 at. % Nb.)

Many aspects of the various transitions in PZT95/5(Nb), including the details of the atomic displacement and changes in lattice parameters involved, remain unresolved. Diffraction studies as functions of P and T can be expected to

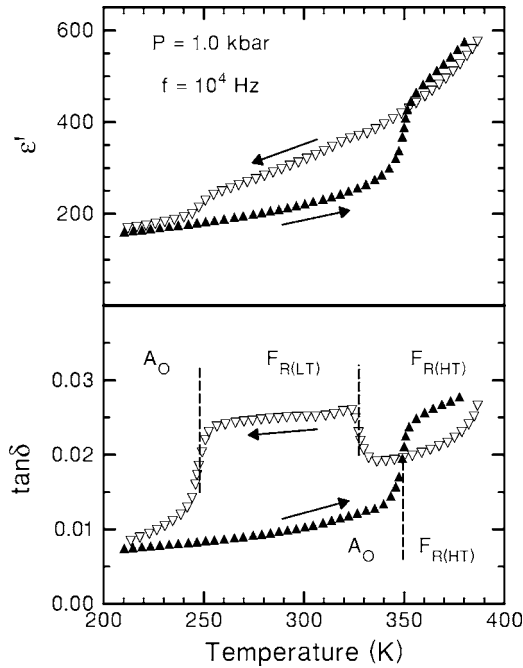


FIG. 1. Variations of ϵ' and $\tan \delta$ for decreasing (open symbols) and subsequent increasing (closed symbols) temperature for the 0.05-cm-thick PZT95/5(2Nb) ceramic disk. The dashed vertical lines denote what we take to be the transition temperatures.

clarify the nature of these transitions and thereby provide a better understanding of the physics. This consideration motivated our present work in which we investigated a particular preparation of PZT95/5(2 at. % Nb) in both ceramic and powder forms with neutron diffraction and dielectric spectroscopy. As will be shown below, the results have shed considerable additional light on the details of the phase behavior of this material.

II. EXPERIMENTAL DETAILS

A. Sample preparation

Oxide powders were precipitated from liquid solutions^{8,9} containing the appropriate quantities of Zr, Ti, Pb, and Nb ions, with 3.75% PbO excess to account for the partial evaporation of Pb during calcining and the subsequent sintering process. The powders were filtered and dried, and then calcined at about 1175 K for 16 h. Rietveld refinements of x-ray diffraction pattern indicated that the as-calcined powder had the $F_{R(LT)}$ structure with a small amount of ZrO_2 phase (4.5 wt %). These quantities might be subject to some uncertainty due to the high absorption of the x-ray radiation compared to that for neutron diffraction. This forms the “powder” sample. The composition of this powder was confirmed by atomic emission spectroscopy, where a slight decrease in Pb concentration (<4%) was observed. The powder was mixed with organic binders (2 wt % acrylic binder solution) to facilitate pressing, dried, pressed into billets, and fired to remove the organic additives. An additional amount of pore former (spherical polymerized methyl methacrylate) was added and mixed with the dry powder to obtain the

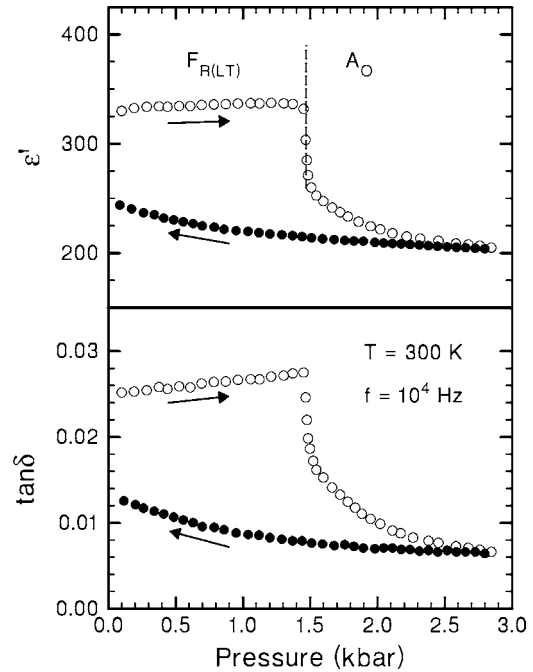


FIG. 2. Variations of ϵ' and $\tan \delta$ for increasing (open symbols) and subsequent decreasing (closed symbols) pressure for the 0.05-cm-thick PZT95/5(2Nb) ceramic disk.

desired electrical and physical properties. The billets were sintered at about 1625 K for 6 h in the presence of calcined powder of composition similar to that of the compact in a double-crucible configuration in order to minimize Pb loss to form the final ceramic. Appropriate sized disks for dielectric (0.4 cm diameter \times 0.05 cm thick and 0.4 cm diameter \times 0.31 cm thick) and neutron diffraction (0.8 cm diameter \times 0.9 cm thick) were cut from the same pellet after the surface layer, which might be slightly Pb deficient, was removed.

The nominal metal composition of the calcined powder was $Pb_{0.9910}(Zr_{0.955}Ti_{0.045})_{0.9820}Nb_{0.018}O_3$ as determined by atomic emission spectroscopy. This composition is designated PZT95/5(2Nb) throughout this paper. It has the $F_{R(LT)}$ phase at ambient conditions. The measured density of this ceramic was 7.312 g/cm³, lower than the theoretical density of 7.989 g/cm³, primarily due to the increased porosity from the pore former.

B. Dielectric measurements

The real (ϵ') and imaginary (ϵ'' or dielectric loss $\tan \delta = \epsilon''/\epsilon'$) components of the dielectric response of our PZT95/5(2Nb) ceramic were measured with an Agilent Model 4284A Precision LCR meter as functions of T (~ 100 – 400 K), P (0–3 kbar), and frequency (10^2 – 10^6 Hz). The electrical contacts were thin films of Cr followed by Au vapor deposited on the large faces of the thin disks. The P and T measurements employed a P cell placed in a cryogenic Dewar; helium gas was the P -transmitting fluid. The P was monitored by the change in resistance of a calibrated manganin coil to better than $\pm 4\%$, and the T was determined to

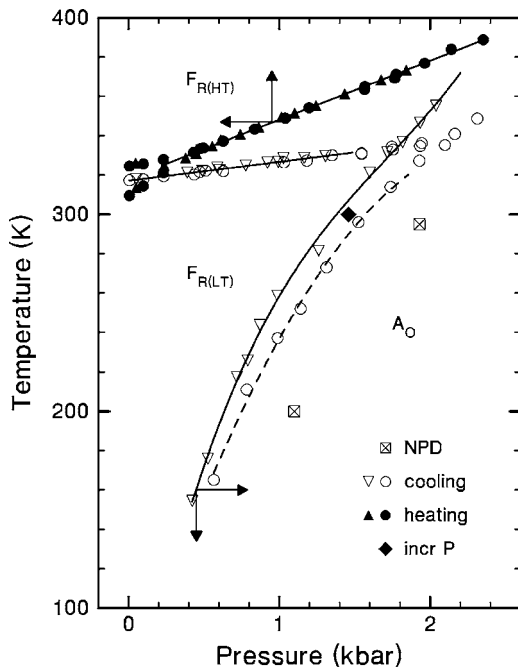


FIG. 3. Partial pressure-temperature phase diagram from dielectric $\tan \delta$ data on the 0.05-cm-thick disk (triangles), 0.31-cm-thick sample (circles), and neutron powder diffraction (squares) experiments.

better than ± 1 K with a chromel/alumel thermocouple mounted adjacent to the sample holder. Typical ac fields (≤ 10 V/cm) employed in the measurements are insufficient to move any domain boundaries of the ferroelectric phases.

C. Neutron powder diffraction measurements

Time-of-flight neutron powder diffraction data were collected on the Special Environment Powder Diffractometer¹⁰ at the Intense Pulsed Neutron Source at the Argonne National Laboratory. Diffraction data were collected as a function of hydrostatic P (0–6.2 kbar) at room T and then at 200 K after an intermediate annealing at 433 K and ambient P for 30 min to recover the $F_{R(LT)}$ phase upon cooling to room T . Hydrostatic P was generated with a helium gas P cell described elsewhere,¹⁰ and cooling was achieved using a closed-cycle helium refrigerator. The P was measured to an accuracy of better than $\pm 4\%$ and the T to an accuracy of ± 1 K. The $\pm 90^\circ$ detector bank data were analyzed using the Rietveld refinement method with the GSAS (EXPGUI) suite.^{11,12} All the instrumental parameters have been determined using a NIST Standard Reference Material silicon standard and kept fixed later. The composition in the refinement was fixed to the nominal one $Pb_{0.9910}(Zr_{0.955}Ti_{0.045})_{0.9820}Nb_{0.018}O_{3.000}$. Neutron scattering lengths used were Pb, 9.405; Zr, 7.16; Ti, -3.438; Nb, 7.054; and O, 5.803 fm. During the course of our refinements on both the ceramic and powder samples, it became evident that peak broadening was occurring, and after a few preliminary trials, anisotropic strain parameters (see below in Sec. III B 2), implemented in the profile function 3 of GSAS, were refined in addition to the usual structural parameters. The

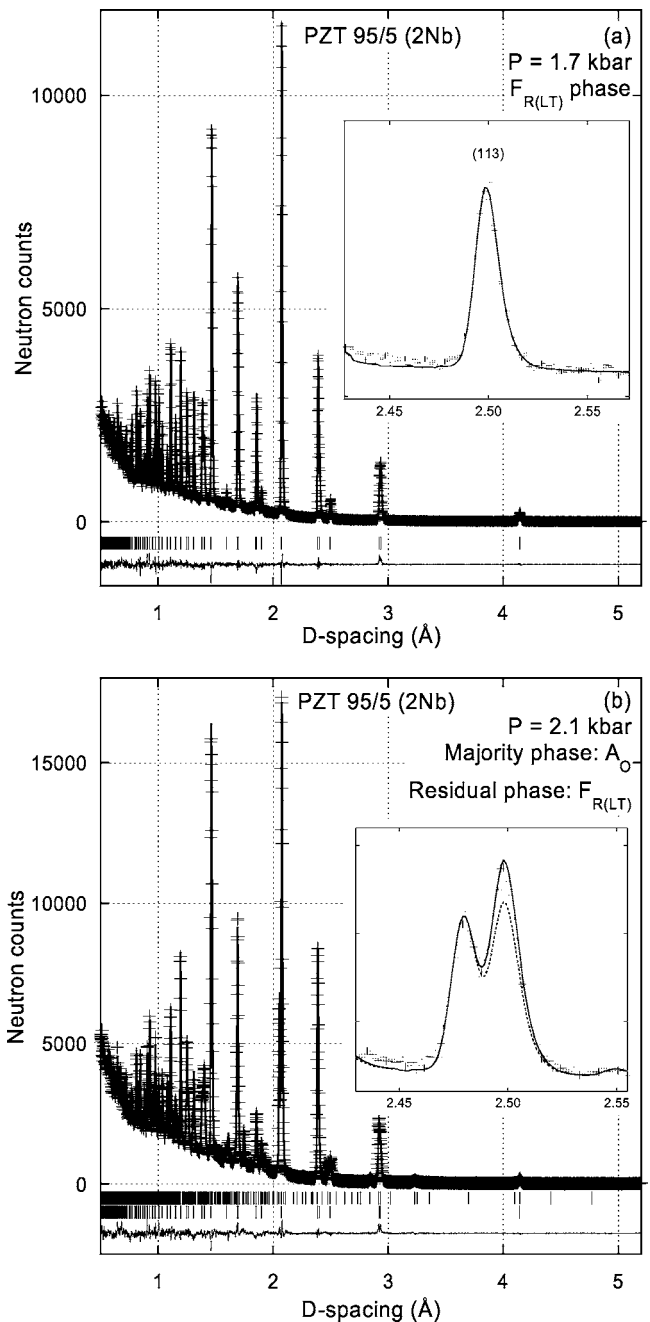


FIG. 4. Observed neutron powder diffraction data and best-fit Rietveld refinement profile for ceramic PZT95/5(2Nb) above (a) and below (b) the phase transition at room temperature. Crosses (+) are the raw data. The solid line is the calculated profile. Tick marks indicate the positions of allowed reflections for $F_{R(LT)}$ and A_O (upper row in two-phase refinement plot) phases. The difference plot on the bottom of each panel is on the same relative scale as the neutron counts. Inset in (a) shows the reflection allowed in $F_{R(LT)}$ $R3c$ space group and not in $F_{R(HT)}$ $R3m$ space group. Inset in (b) shows the results of $A_O + F_{R(LT)}$ (solid line, $R_p = 3.33\%$, $R_{wp} = 5.13\%$, $\chi^2 = 2.36$) and $A_O + F_{R(HT)}$ (dashed line, $R_p = 3.61\%$, $R_{wp} = 5.40\%$, $\chi^2 = 2.62$) refinement. Better refinement in the former case is due to the contribution of (113) reflection of the $F_{R(LT)}$ $R3c$ phase, which is not allowed in the $F_{R(HT)}$ $R3m$ phase.

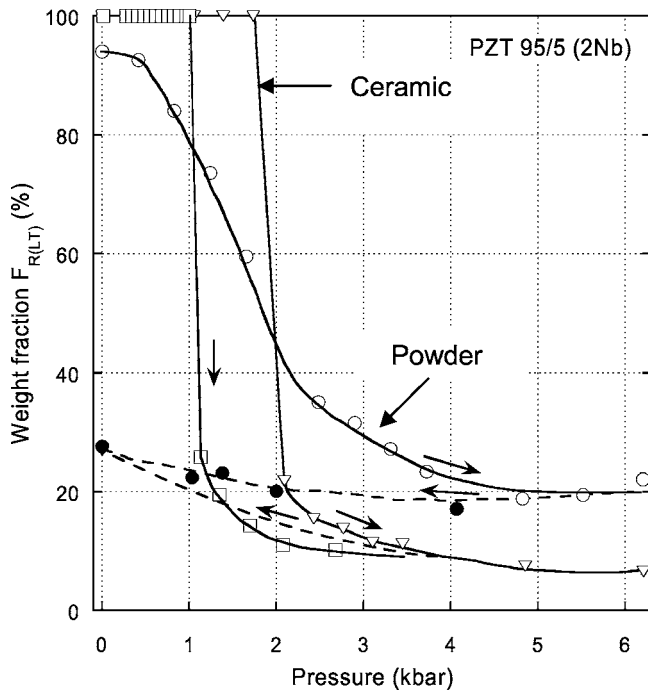


FIG. 5. Weight percent of $F_{R(LT)}$ phase as a function of increasing hydrostatic pressure for powder sample at 295 K (open circles) and ceramic sample at 295 K (open triangles) and at 200 K (open squares). These symbols are filled for decreasing pressure. (Note the filled triangle is at the same weight fraction as the filled circle; the corresponding point at 200 K was not determined.) Solid (dashed) lines are an aid to follow data points for increasing (decreasing) pressure. The remaining weight fraction is the A_O phase.

structural models for the Rietveld refinement of the data collected at ambient T and P were taken from the recent reinvestigations of rhombohedral¹³ and orthorhombic¹⁴ PZT phases.

III. RESULTS AND DISCUSSION

A. Dielectric properties and temperature-pressure phase diagram

Being very near the $F_{R(LT)}-A_O$ phase boundary, at 295 K, PZT95/5(2Nb) is known³ to transform from the $F_{R(LT)}$ phase to the A_O phase under modest hydrostatic P . We have developed a partial T - P phase diagram for our sample from dielectric measurements.

Figure 1 shows the T dependences of ϵ' and $\tan \delta$ for a 0.05-cm-thick ceramic disk sample at 1.0 kbar measured at 10^4 Hz on cooling from 390 K (open symbols) and subsequent warming from 210 K (closed symbols). The data were recorded while heating or cooling at approximately 1.5 K/min. The ϵ' cooling data show a subtle change near 330 K and significant decrease near 250 K; in contrast, the $\tan \delta$ data have a pronounced increase with decreasing T near 330 K followed by a large decrease near 250 K. These changes in dielectric loss reflect the $F_{R(HT)}-F_{R(LT)}$ and $F_{R(LT)}-A_O$ phase transitions, respectively; the midpoints of the large $\tan \delta$ changes, shown by dashed lines in Fig. 1,

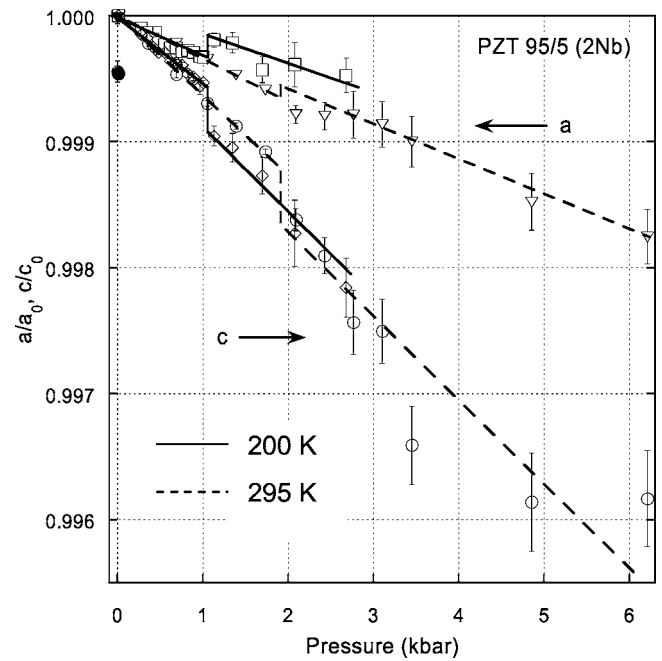


FIG. 6. Relative change in the a and c cell parameters (hexagonal basis) of the $F_{R(LT)}$ phase. Solid lines through open squares (a axis) and open diamonds (c axis) are used for 200 K data; dashed lines through open triangles and circles for the corresponding 295 K data. Filled symbols are ambient points after pressure release.

were chosen as the respective transition temperatures. Both the ϵ' and $\tan \delta$ heating data show a substantial rise near 350 K, reflecting the $A_O-F_{R(HT)}$ phase transition. Similar data were obtained with a 0.31-cm-thick disk. The $F_{R(HT)}-F_{R(LT)}$ transition near 330 K on cooling is in good agreement with that determined by interpolating Garcia *et al.*'s⁵ points, including his 1 wt % Nb_2O_5 (= to 2.6 at. % Nb), near our 1.8 at. % determined composition. Our larger temperature hysteresis results from our cooling into the A_O phase, whereas in Garcia *et al.*'s study the sample remained above the A_O transition.

Figure 2 shows the P dependences of ϵ' and $\tan \delta$ at 300 K measured at 10^4 Hz on the same disk. The dielectric data were recorded after stepwise changes in P ; both increasing and decreasing P runs required approximately 2 h. To ensure that the sample was initially in the $F_{R(LT)}$ phase and did not contain any A_O second phase, it was heated to 390 K under 50 bar and then cooled to 300 K prior to applying pressure. With increasing P (open symbols) there is a rapid decrease in both ϵ' and $\tan \delta$ near 1.5 kbar, reflecting the $F_{R(LT)}-A_O$ transition. Once in the A_O phase, the sample exhibits a large hysteresis on lowering the P (closed symbols in Fig. 2). There is no evidence in either ϵ' or $\tan \delta$ for a reverse transition to a FE phase during the P release at 300 K; the ceramic sample remains in the A_O phase. However, our previous studies of similar ceramic samples have shown a slow recovery of the $F_{R(LT)}$ phase over several days at ambient P and T . Full recovery of the $F_{R(LT)}$ phase requires heating the ceramic above 350 K, i.e., to the $F_{R(HT)}$ phase, and then lowering T back to room T .

The sharpness of the transition in both $\epsilon'(P)$ and $\tan \delta(P)$ attests to the high quality and compositional uniformity of

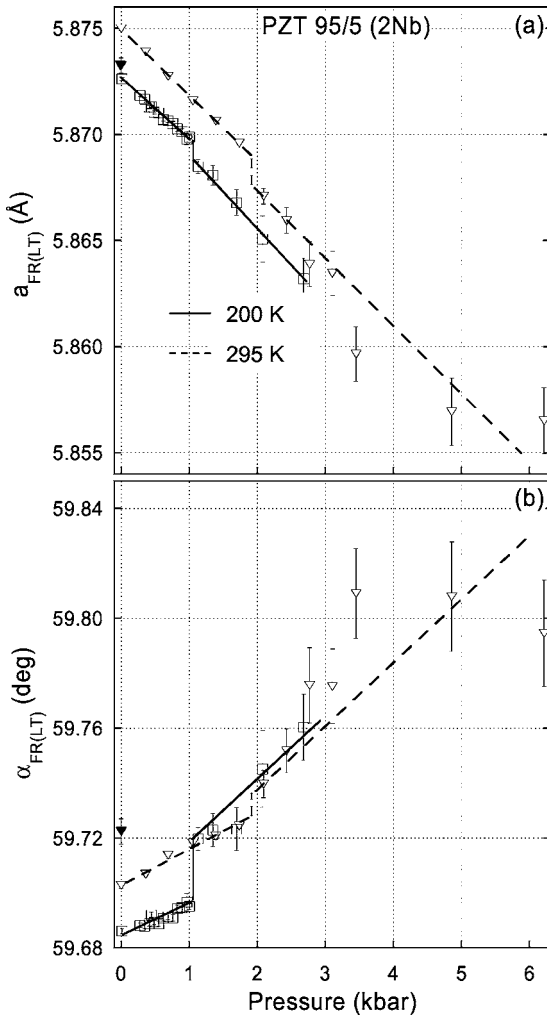


FIG. 7. Relative change in the a and α cell parameters (rhombohedral setting) of the $F_{R(LT)}$ phase. Solid lines through 200 K data (open squares); dashed lines 295 K data (open diamonds). Filled symbols are ambient points after pressure release for 295 K.

the sample used. It is also seen that after the initial drop in ϵ' and $\tan \delta$ at 1.5 kbar there is a long tailing off in these properties with increasing P . As we shall show later, this tailing off is associated with the fact that although a large fraction of the $F_{R(LT)}$ phase transforms to A_O at 1.5 kbar, a much higher P is needed to complete the transformation. It should also be noted here that whereas both ϵ' and $\tan \delta$ exhibited small frequency dispersion in both the FE and A_O phases, the transition P was independent of frequency.

Figure 3 shows a partial T - P phase diagram for the two ceramic samples, triangles for the 0.05-cm-thick disk, and circles for the 0.31-cm-thick disk. This diagram is qualitatively similar to that determined by Fritz and Keck,³ but there are significant quantitative, sample-dependent differences primarily due to small Pb concentration differences.^{7,9} We felt it important to determine this diagram for the same PZT95/5(2Nb) material used for our neutron diffraction data to be presented in Sec. III B below. All of the data points in Fig. 3, except for the solid diamond at 300 K and 1.5 kbar, were determined from $\tan \delta(T)$ isobars as in Fig. 1. The midpoint T for each change in $\tan \delta$ and the corresponding P

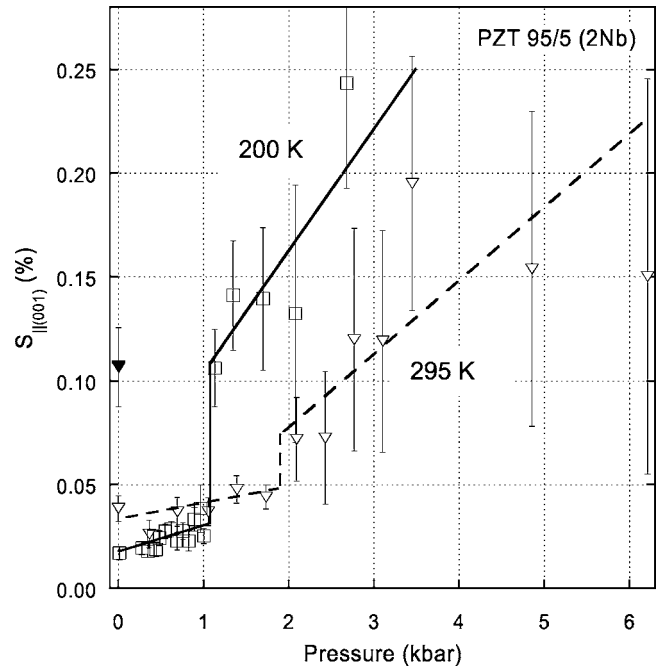


FIG. 8. Anisotropic strain for the $F_{R(LT)}$ phase in the ceramic sample at 295 K (triangles) and 200 K (squares) as a function of pressure. Note the abrupt increase slightly above 1.1 (1.9) kbar at the $F_{R(LT)}$ - A_O phase transitions for 200 (295) K data. The strain is retained on pressure release at 295 K (filled triangle).

(dashed vertical lines in Fig. 1) were used to construct Fig. 3.

All transitions in Fig. 3 exhibit marked T or P hysteresis. The open triangles and circles indicate a boundary that is crossed by increasing P or by decreasing T (indicated by the arrows). Similarly, the solid triangles and circles indicate a boundary that is crossed by increasing T or decreasing P . Note that there is a large thermal hysteresis associated with the $F_{R(LT)}$ - A_O transition. For example, whereas the lower phase boundary denoted by the open symbols represents the $F_{R(LT)}$ - A_O transition on cooling at fixed P , the reverse A_O - $F_{R(LT)}$ transition on warming is only observed near 1 bar and 310 K. At higher pressures, the A_O phase transforms directly to the $F_{R(HT)}$ phase with increasing T . The solid diamond datum point at 300 K and 1.5 kbar on the lower phase boundary in Fig. 3 was determined from the isothermal, increasing- P scan in Fig. 2, thereby showing good agreement between isothermal and isobaric measurements. Also included on this figure are two open squares at 200 and 295 K which correspond to the $F_{R(LT)}$ - A_O phase transition as determined from neutron diffraction spectra on increasing P (see Sec. III B 2).

Our initial dielectric measurements were performed on the 0.4-cm-diameter \times 0.05-cm-thick disk (triangles in Fig. 3). Subsequently, the neutron diffraction data on the 0.8-cm-diameter \times 0.9-cm-thick disks showed that the $F_{R(LT)}$ - A_O transition at 200 and 295 K in Fig. 3 occurs at pressures roughly 0.5 kbar above the corresponding values determined by dielectric measurements on the 0.05-cm-thin disk. In searching for an explanation of this discrepancy, we ruled out any substantial error in the respective P determina-

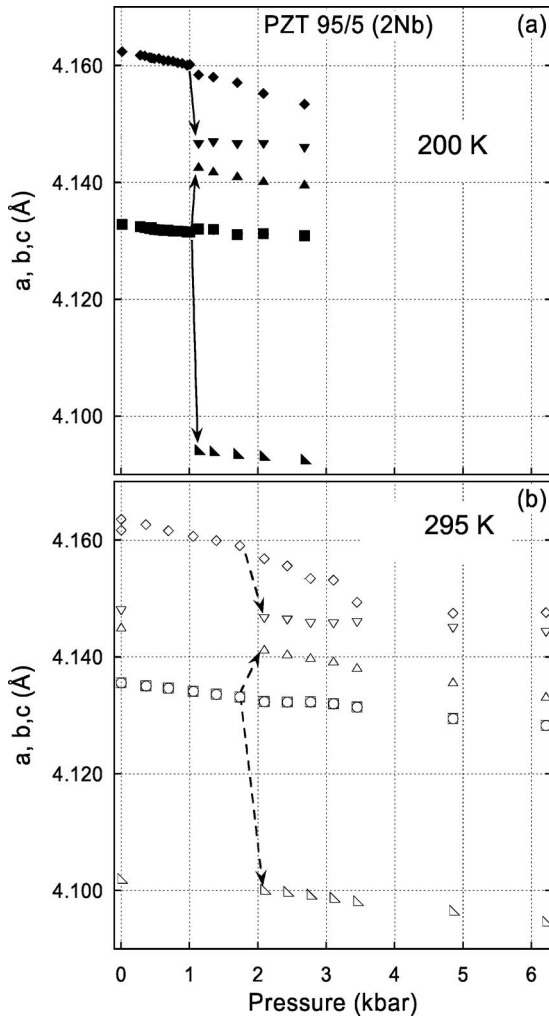


FIG. 9. Reduced a, b , and c cell parameters for the $F_{R(LT)}$ (circles, squares, and diamonds) and A_O (upward, downward, and right triangles) phases: (a) at 200 K (filled symbols; solid arrows) and (b) at 295 K (open symbols; dashed arrows). Values at 295 K on pressure release to ambient are also shown.

tions, as the P in both apparatuses is accurate to $\pm 4\%$. An alternate possibility involves the large difference in the smallest sample dimension, the disk thickness, 0.05 cm for the dielectric sample versus 0.9 cm for the neutron diffraction sample. To investigate this further, a second dielectric sample was cut from the same ceramic pellet as for the neutron measurements with an identical diameter (0.4 cm) to the 0.05-cm-thick sample, but with a thickness of 0.31 cm. The data for the 0.31-cm-thick sample are shown as circles in Fig. 3, with the solid and open circles representing heating and cooling transitions. While two of the three phase boundaries in Fig. 3 show no thickness dependence, there is a significant shift in the $F_{R(LT)}-A_O$ transition; it occurs at roughly 0.15 kbar greater P for a given T in the thicker sample. An extrapolation of this result to the 0.9 cm thickness of the neutron diffraction sample interestingly predicts an ~ 0.5 kbar higher transition P than for the 0.05-cm-thick dielectric sample, consistent with the data in Fig. 3. See Sec. III B for discussion.

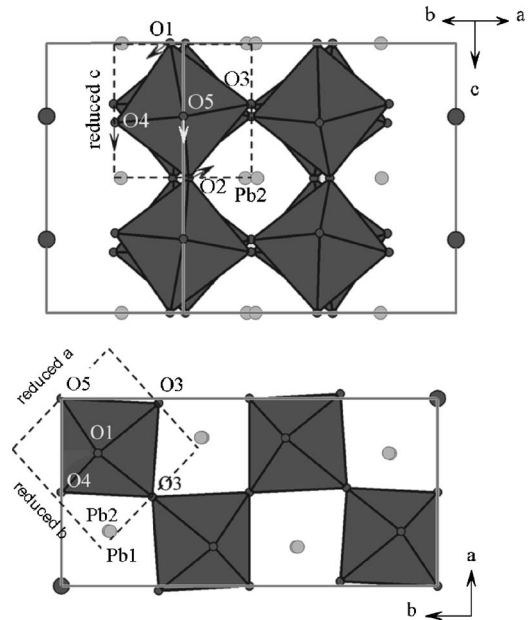


FIG. 10. Relationship of the reduced cell parameters to the normal orthorhombic cell of the A_O structure: (top) projection on 210 of the A_O cell; (bottom) projection on 001 of only the upper half of the unit cell.

B. Neutron diffraction results

1. Diffraction profiles

The analysis of over 50 P and T data refinement sets for our ceramic and powder samples showed that a difference in sample preparation resulted in the difference in the sample phase composition. While our ceramic sample is pure $F_{R(LT)}$ phase with no evidence of ZrO_2 , probably due to the higher- T sintering process, our powder sample contains both 4.2 (5) wt % A_O phase and 0.8 (1) wt % ZrO_2 , presumably because of PbO loss from the surface of powder grains. Due to the very low ZrO_2 content, the structural parameters of monoclinic zirconia were fixed according to Maistrelli *et al.*,¹⁵ with the phase fraction being the only variable. For the most part, detailed results are presented only for the ceramic sample. Comments are made on the powder results whenever they complement those of the ceramic results.

Figure 4 shows typical data sets of neutron diffraction spectra and best-fit Rietveld refinement profiles for our ceramic sample at 1.7 and 2.1 kbar at 295 K. These pressures are just below and just above the $F_{R(LT)}-A_O$ phase transition (see Fig. 5). The fits shown in the insets are discussed below. The refinements of all data sets (approximately 50) show similar agreement, with R_p, R_{wp} , and χ^2 values being 2.5–3.5 %, 3.5–7.5 %, and 1.5–2.3, respectively.

2. $F_{R(LT)}-A_O$ phase transition

Figure 5 shows the $F_{R(LT)}-A_O$ phase transition deduced from neutron diffraction data on the ceramic and powder samples. Plotted in Fig. 5 is the weight fraction of the $F_{R(LT)}$ phase as a function of P at 295 and 200 K. It is seen that the transition in the ceramic is sharp and occurs at 1.9 and 1.1

TABLE I. Refined structural parameters for $F_{R(LT)}$ phase in ceramic sample of PZT95/5(2Nb) at 295 and 200 K. Space group $R3c$ (no. 161), with Pb at $6a(0,0,z)$, Zr (Ti) at $6a(0,0,z)$, and O at $18b(x,y,z=1/12)$. Numbers in parentheses are statistical standard deviations of the last significant digit. Dashes indicate that the corresponding parameter was not refined due to low fraction of $F_{R(LT)}$ phase.

	200					295				
	0	1.0	1.1	2.7	0	1.7	2.1	6.2	0 ^a	
P (kbar)										
a (Å)	5.84473(6)	5.84280(6)	5.8436(3)	5.8419(8)	5.84858(7)	5.84513(6)	5.8440(4)	5.8383(13)	5.8486(4)	
c (Å)	14.4189(3)	14.4113(3)	14.4052(11)	14.388(3)	14.4230(3)	14.4074(3)	14.400(1)	14.368(6)	14.417(1)	
z (Pb)	0.2846(1)	0.2842(1)	0.2830(4)	0.281(1)	0.2825(2)	0.2819(1)	0.2815(5)	0.273(3)	0.2815(5)	
U_{11} (Pb)(Å ²)	0.0120(4)	0.0113(5)	0.0113(—)	0.0113(—)	0.0193(6)	0.0173(5)	0.0173(—)	0.0173(—)	0.0193(—)	
U_{33} (Pb)(Å ²)	0.0061(5)	0.0054(6)	0.0054(—)	0.0054(—)	0.0084(8)	0.0082(7)	0.0082(—)	0.0082(—)	0.0084(—)	
z (Zr/Ti)	0.0141(1)	0.0137(2)	0.0142(5)	0.016(1)	0.0128(2)	0.0125(2)	0.0129(6)	0.036(3)	0.0133(5)	
U_{iso} (Zr/Ti)(Å ²)	0.0049(3)	0.0049(3)	0.0049(—)	0.0049(—)	0.0061(3)	0.0068(3)	0.0068(—)	0.0068(—)	0.0061(—)	
x (O)	0.1396(2)	0.1388(2)	0.1426(10)	0.149(3)	0.1426(3)	0.1408(3)	0.1483(12)	0.172(5)	0.1485(12)	
y (O)	0.3480(3)	0.3480(3)	0.3547(9)	0.365(2)	0.3473(3)	0.3473(3)	0.3573(10)	0.389(4)	0.3536(10)	
U_{11} (O)(Å ²)	0.0140(7)	0.0131(8)	0.0131(—)	0.0131(—)	0.0188(10)	0.0182(9)	0.0182(—)	0.0182(—)	0.0188(—)	
U_{22} (O)(Å ²)	0.0094(7)	0.0110(8)	0.0110(—)	0.0110(—)	0.0105(8)	0.0112(8)	0.0112(—)	0.0112(—)	0.0105(—)	
U_{33} (O)(Å ²)	0.0098(7)	0.0119(8)	0.0119(—)	0.0119(—)	0.020(1)	0.021(1)	0.021(—)	0.021(—)	0.020(—)	
U_{12} (O)(Å ²)	0.0043(8)	0.0049(9)	0.0049(—)	0.0049(—)	0.0049(11)	0.0062(10)	0.0062(—)	0.0062(—)	0.0049(—)	
U_{13} (O)(Å ²)	-0.0013(6)	-0.0012(7)	-0.0012(—)	-0.0012(—)	-0.0015(10)	-0.0011(9)	-0.0011(—)	-0.0011(—)	-0.0015(—)	
U_{23} (O)(Å ²)	-0.0041(5)	-0.0039(5)	-0.0039(—)	-0.0039(—)	-0.0063(6)	-0.0056(6)	-0.0056(—)	-0.0056(—)	-0.0063(—)	
R_p (%)	3.30	3.60	3.34	3.39	3.94	3.57	3.33	4.01	3.85	
R_{wp} (%)	6.77	7.40	5.97	6.39	6.65	5.81	5.13	6.45	6.27	
χ^2	1.59	1.50	1.77	1.70	1.52	1.53	2.36	1.49	1.54	

^aAfter pressure release.

kbar (taken as the midpoint pressures for the large drops in weight fraction) at 295 and 200 K, respectively. These points are shown by the open squares on the phase diagram, Fig. 3. Clearly both points fall significantly to the right of the $F_{R(LT)}-A_O$ phase boundary determined from the dielectric measurements on the 0.05-cm-thick disks, raising a question about the difference between the dielectric and neutron measurements. In both experiments, helium was the P -transmitting medium, so the applied P is hydrostatic. Additionally, the P calibrations for both apparatuses are accurate to better than $\pm 4\%$, and for both experiments the onset and most of the transition are quite sharp, ruling out significant compositional inhomogeneities.

While this observed dependence of the $F_{R(LT)}-A_O$ transition pressure on sample size may seem strange, consideration of the nature of the present sample sheds light on the issue. The ceramic samples used are made up of randomly oriented, anisotropic grains. Applying hydrostatic pressure to the outside of such samples results in a complex stress distribution between and within the grains, especially when the grains are exposed to conditions where they would normally undergo a phase transition that involves anisotropic axial deformation of the lattice. It is not difficult to envision that under such circumstances clamping of grains by differently oriented adjoining grains could occur and hinder the grains' deformations and thereby the phase transition. It is also not difficult to envision that this effect would be more pronounced the more massive the sample. Indeed, the neutron diffraction data to be presented below clearly show the exis-

tence of relatively large anisotropic strains and stresses associated with the FE-to-AFE transition. It also follows from these arguments that when the transition involves little or no strain, then the effect of sample size is essentially absent. This is the case for the $F_{R(LT)}-F_{R(HT)}$ transition in Fig 3. In this case the transition is subtle involving the counterrotations of adjacent oxygen octahedral and very minor lattice strain. The $F_{R(LT)}-A_O$ transition, on the other hand, is accompanied by large lattice strain. One of the present authors (P.Y.) has recently measured these linear transformational strains (during cooling cycles on a ceramic sample of PZT95/5 without Nb addition), and they are -0.2265% for the $F_{R(LT)}-A_O$ transition and -0.0178% for the $F_{R(HT)}-F_{R(LT)}$ transition.

This is part of the reason that the transition of the powder sample (Fig. 5) is so spread out. It is also consistent with the observed disk thickness dependence noted in the dielectric measurements. Note that the midpoint of the transition in the

TABLE II. Atomic coordinates of $F_{R(LT)}$ $R3c$ phase (hexagonal setting) in terms of structural parameters s, t, d , and e , following Megaw and Darlington (Ref. 20).

Atom	x	y	z
Pb	0	0	$s+1/4$
Zr/Ti	0	0	t
O	$1/6-2e-2d$	$1/3-4d$	$1/12$

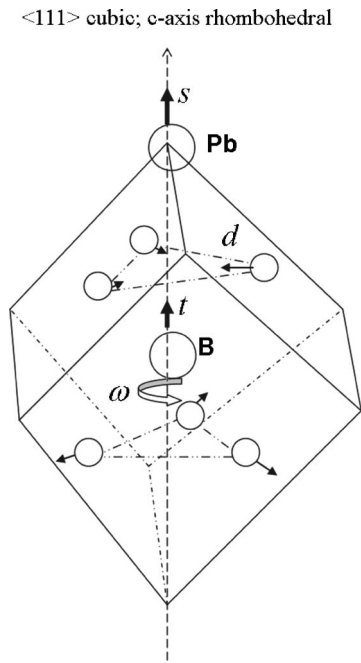


FIG. 11. Primitive cubic cell shown with $\langle 111 \rangle$ vertical. The actual rhombohedral cell is twice as big with its c axis along $\langle 111 \rangle$. The positional parameters from the ideal cubic positions (see Table II) are s and t for Pb and B- site ions, respectively, along $\langle 111 \rangle$, d and e , schematically shown as arrows, for the motion of the oxide ions relative to (in or out) and about the $\langle 111 \rangle$ axis, respectively. (ω is defined in the text.)

powder occurs at ~ 60 wt % and at ~ 1.5 kbar, substantially below the midpoint of the ceramic at ~ 2.1 kbar. This circumstance will become clearer below when we present details of the P -induced changes in cell parameters.

It is clear from Fig. 5 that the $F_{R(LT)}-A_O$ transition is certainly not complete after the initial sharp drop. The results show that after the initial drop, 20% of the sample remains as a minority $F_{R(LT)}$ phase together with the A_O phase. This minority phase transforms gradually to A_O with increasing P , but even at 6.2 kbar (or three times the initial transition P) remarkably about 8% of the sample remains in the $F_{R(LT)}$ phase. Further insights into this rather unusual behavior are provided by analysis of the neutron data of the residual $F_{R(LT)}$ phase that is dispersed in the majority high- P A_O phase, as will be discussed in Sec. III C.

It can also be seen from Fig. 5 that the transformation is largely irreversible on releasing the P at room T , in agreement with dielectric data in Figs. 2 and 3 and with earlier results on PZTs.^{3,16} Our diffraction data show that after releasing the P to 1 bar only $\sim 27\%$ of the sample was in the $F_{R(LT)}$ phase.

Figure 5 also shows results on a powder PZT95/5(2Nb) sample. In this case the powder had $\sim 5\%$ of the A_O phase to start with, and it is seen that the $F_{R(LT)}-A_O$ transition is continuous and incomplete at 6 kbar, where 20% of the sample retains the low- P $F_{R(LT)}$ phase. Again the transformation is irreversible upon releasing the P . The recovered powder sample at 1 bar had $\sim 27\%$ $F_{R(LT)}$ phase, the same as for the ceramic sample. Note that the recovered powder and ceramic

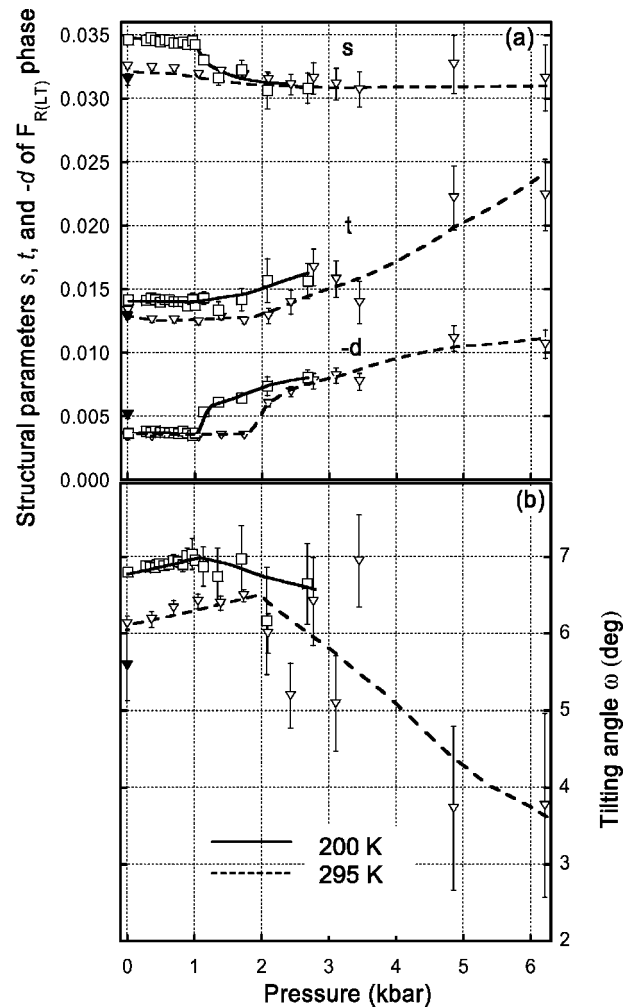


FIG. 12. Structural parameters s, t, d (top) and tilt angle ω (bottom) for the $F_{R(LT)}$ phase as a function of pressure. Solid (dashed) lines are visual aids passing through the 200 (295) K values. Note the discontinuities at the phase boundary and that negative values of d are shown.

points superimpose on each other at 1 bar in Fig. 5.

Careful inspection of the lattice parameters of the $F_{R(LT)}$ phase above and below the transition, i.e., the starting material compared with the remaining nontransformed material reveals a remarkable behavior. On a hexagonal basis, the a and c axes, of course, contract with increasing P as expected in the low- P $F_{R(LT)}$ phase, but exhibit the unusual behavior shown at and above the transition where the $F_{R(LT)}$ exists as a minority phase. Specifically, the a axis actually expands while the c axis contracts (Fig. 6) by a large enough amount at the transition to result in an overall reduction of the $F_{R(LT)}$ cell volume. This is more apparent in the 200 K data; however, it can also be seen in the 295 K data highlighted by the dashed lines. This appears to be very much like a first-order transition. Above the transition both lattice parameters contract with P , as expected, with c showing a much larger contraction. The large error bars above the transition result from the reduced amount of $F_{R(LT)}$ phase. Because of the first-order nature of this transition, one needs to establish that

TABLE III. Refined structural parameters for A_O phase in ceramic sample. Space group $Pbam$ (no. 55), with Pb1 and O1 at $4g(x, y, 0)$, Pb2 and O2 at $4h(x, y, 1/2)$, Zr (Ti) and O3 at $8i(x, y, z)$, O4 at $4f(1/2, 0, z)$, and O5 at $4e(0, 1/2, z)$. Numbers in parentheses are statistical standard deviations of the last significant digit.

	T (K)					
	200			295		
P (kbar)	1.1	2.7	2.1	6.2	0 ^a	
a (Å)	5.8587(3)	5.8544(2)	5.8567(3)	5.8451(2)	5.8620(3)	
b (Å)	11.7280(7)	11.7261(6)	11.7282(7)	11.7217(6)	11.7319(8)	
c (Å)	8.1885(2)	8.1853(2)	8.2004(2)	8.1896(2)	8.2042(2)	
x (Pb1)	0.7074(9)	0.7088(8)	0.7099(10)	0.7122(9)	0.7081(12)	
y (Pb1)	0.1293(4)	0.1296(4)	0.1290(5)	0.1302(5)	0.1292(6)	
U_{iso} (Pb1)(Å ²)	0.0083(11)	0.0088(10)	0.013(1)	0.013(1)	0.015(2)	
x (Pb2)	0.7065(9)	0.7074(8)	0.7148(10)	0.7116(9)	0.7080(12)	
y (Pb2)	0.1249(4)	0.1248(4)	0.1259(5)	0.1260(5)	0.1261(6)	
U_{iso} (Pb2)(Å ²)	0.011(1)	0.012(1)	0.022(2)	0.019(1)	0.015(2)	
x (Zr/Ti)	0.2423(5)	0.2422(4)	0.2431(5)	0.2431(7)	0.2423(6)	
y (Zr/Ti)	0.1217(5)	0.1214(4)	0.1217(5)	0.1232(5)	0.1223(6)	
z (Zr/Ti)	0.2548(8)	0.2560(5)	0.2549(7)	0.2538(7)	0.2547(8)	
U_{iso} (Zr/Ti)(Å ²)	0.0034(5)	0.0028(4)	0.0045(4)	0.0045(4)	0.0045(5)	
x (O1)	0.2909(14)	0.2902(11)	0.2844(13)	0.2907(14)	0.2879(16)	
y (O1)	0.0974(9)	0.0961(7)	0.0966(8)	0.0971(9)	0.0993(11)	
U_{iso} (O1)(Å ²)	0.015(2)	0.012(1)	0.013(1)	0.019(2)	0.016(2)	
x (O2)	0.2669(12)	0.2692(11)	0.2681(12)	0.2649(12)	0.2676(15)	
y (O2)	0.1547(8)	0.1535(7)	0.1523(8)	0.1519(8)	0.1536(10)	
U_{iso} (O2)(Å ²)	0.0056(15)	0.0099(14)	0.013(2)	0.0071(15)	0.011(2)	
x (O3)	0.0240(9)	0.0248(8)	0.0229(10)	0.0255(10)	0.0236(12)	
y (O3)	0.2574(3)	0.2585(3)	0.2569(3)	0.2584(3)	0.2580(4)	
z (O3)	0.2254(8)	0.2251(7)	0.2268(8)	0.2270(7)	0.2277(8)	
U_{iso} (O3)(Å ²)	0.015(1)	0.014(1)	0.019(1)	0.017(1)	0.020(2)	
z (O4)	0.2944(8)	0.2947(7)	0.2931(8)	0.2952(8)	0.2923(9)	
U_{iso} (O4)(Å ²)	0.0068(12)	0.0075(11)	0.0098(12)	0.0090(12)	0.0098(14)	
z (O5)	0.2709(11)	0.2715(9)	0.2698(10)	0.2730(9)	0.2722(11)	
U_{iso} (O5)(Å ²)	0.012(1)	0.013(1)	0.017(1)	0.014(1)	0.012(2)	

^aAfter pressure release.

the transition does not involve the $F_{R(\text{HT})}$ space group. The insets in Fig. 4 show (a) a peak forbidden in $F_{R(\text{HT})}$ before the transition, and (b) that peak in combination with two other peaks for the A_O phase. Better agreement in the refinement is achieved with a contribution of the (113) reflection of the $F_{R(\text{LT})}$ phase, which is not allowed in the $F_{R(\text{HT})}$ phase. Figure 7 gives the rhombohedral basis cell parameters allowing one to easily assess that, for both 200 and 295 K, the lattice changes with increasing P are toward a cubic lattice.

Evidence for a high degree of clamping of the grains in the $F_{R(\text{LT})}$ phase in the ceramic sample can be seen in Fig. 8. Plotted is the strain along $\langle 001 \rangle$, S_{\parallel} , for both the $F_{R(\text{LT})}$ phase (below ~ 1 kbar) and for the remaining $F_{R(\text{LT})}$ grains that exist as a minority phase in the A_O phase (above 1 kbar). This strain is determined by the GSAS refinement of two peak profile broadening parameters γ_1 and γ_{1e} , perpendicular and parallel to $\langle 001 \rangle$, respectively, from which the anisotropic strain is determined.^{11,17} In the present case, γ_1 remained

within 1 e.s.d. from 0 in all our refinements; thus S_{\parallel} is directly related to γ_{1e} . Note that the strain nearly doubles with increasing P in the low- P $F_{R(\text{LT})}$ phase, takes a much larger and sharp increase at the transition and continues to exhibit a remarkable increase for the minority $F_{R(\text{LT})}$ grains in the high- P A_O phase. Figure 8 thus provides direct evidence that the $F_{R(\text{LT})}$ domains experience high anisotropic stresses and inhomogeneous strains from their surroundings in both the low- and high- P phases.

Turning our attention to the majority high- P A_O phase, we see in Fig. 9 that the above mentioned (possibly first-order) transition in the $F_{R(\text{LT})}$ phase involves smaller cell parameter changes than those in the A_O phase. Figure 9 employs cell parameters normalized to those for one formula unit per cell (the same as that of the cubic phase). At the $F_{R(\text{LT})}$ - A_O phase transition, the reduced orthorhombic a cell parameter decreases abruptly by $\sim 0.4\%$, the b parameter increases by $\sim 0.3\%$, and the c parameter decreases by $\sim 1\%$ for both the 200 and 295 K data. It is this large anisotropic contraction

that leads to the abrupt strain broadening at the transition mentioned above (Fig. 8). The reduced normalized cell parameters in Fig. 9 may be better visualized with respect to the usual orthorhombic cell parameters by using the dashed cell shown in Fig. 10. One of the axes (the smallest one along c) experiences compression about three times larger than the other axis due to the buckling of the octahedra in the structure. Thus, the distortion upon transforming to the A_O phase is very anisotropic. In a ceramic sample where particles are sintered together in random orientations, this will lead to large grain-interaction stresses. The system can relieve some of this stress by leaving a fraction (in our case about 10%) of the sample in the $F_{R(LT)}$ phase. The resulting minority $F_{R(LT)}$ phase in the majority A_O phase is, thus, highly distorted. Nevertheless, this is where the total energy of the “microcomposite” system is minimized. Further, the system with its small increases in the a parameter of the $F_{R(LT)}$ phase and the b parameter of the A_O phase and larger decreases in the remaining cell parameters becomes sensitive to the total loads transmitted by their neighboring domains so as to be influenced by the thickness of the ceramic sample.

C. Details of the atomic structures

The phase transitions in the PZT's have their origin in small ionic displacements. A quick summary of such displacements follows. The cubic to $F_{R(HT)}$ transition essentially involves a stretching along one threefold axis of the cubic cell, i.e., the cubic cell angle becomes slightly less than 90° (less than 60° if the reduced cell is used), with the Pb, B -site, and O ions shifting from the cubic symmetry sites, the first two along and the latter normal to the threefold axis (preserving or remaining on the mirror plane). (The displacements are sometimes designated by the structural parameters s, t, d and e or $\omega=0$; see below.) The $F_{R(HT)}-F_{R(LT)}$ transition removes the requirement that the O ion remains on the mirror plane, a motion which translates to e or ω having a finite value; the resulting symmetry operation requires doubling the length of the cell along the threefold axis. Finally, at the $F_{R(LT)}-A_O$ transition, the cell shrinks along this original threefold axis and distorts normal to it, by expanding in one direction and contracting normal to that direction. This transformation abruptly shifts the O octahedra about the B -site ions, so that a corrugated or buckled structure occurs along one direction (crystallographic convention rules label this as the orthorhombic b axis; Fig. 10, top).

Let us now consider in more detail the structural results for the $F_{R(LT)}$ phase. Table I gives our refined structural parameters for this phase at 1 bar and at pressures below and above the $F_{R(LT)}-A_O$ phase transition, at 200 and 295 K, as well as for the recovered sample at 1 bar and 295 K. This table covers the P range of our experiments on the $F_{R(LT)}$ phase.

Traditionally, the rhombohedral phase derived from the cubic perovskite by antiphase tilting (rotation and distortion) of oxygen octahedra about $\langle 111 \rangle_p$ and cation shifts along $\langle 111 \rangle_p$ (i.e., $a^-a^-a^-$ tilt system) is described by the notation of Glazer.^{18,19} This more easily visualized system is de-

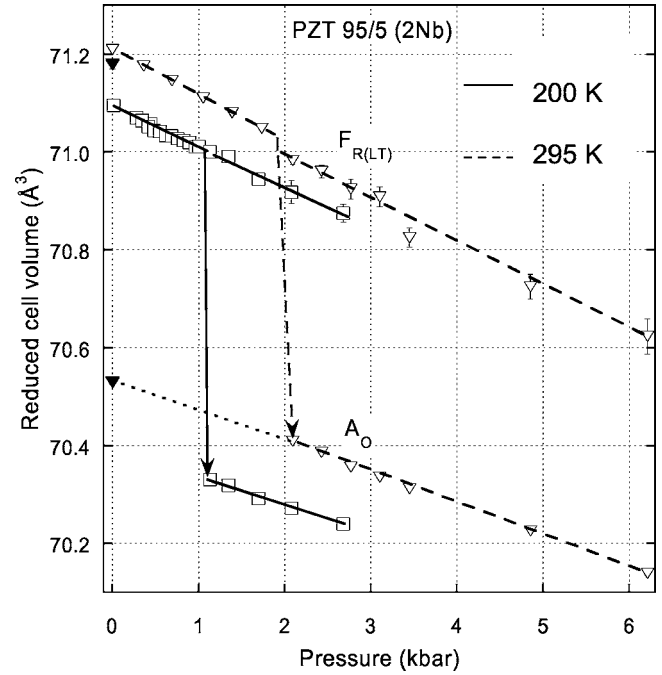


FIG. 13. Normalized cell volume as a function of pressure. Solid lines through 200 K values (open squares); dashed through 295 K values (open triangles), with return to ambient pressure (filled). Note the smaller cell for the A_O phase compared to the $F_{R(LT)}$ phase.

scribed by four parameters related to the atomic coordinates as presented in Table II. Figure 11 shows these parameters relative to a schematic of the cell. Parameters s and t measure the Pb and B -site cation displacements, respectively, along $\langle 111 \rangle_p$ from the ideal cubic cell positions with an origin chosen to be midpoint between opposite faces of an oxygen octahedron. The parameter d describes the way an octahedron is distorted, keeping the threefold symmetry axis, but making the upper and lower faces different in size. The parameter e describes the rotation of an octahedron about the

TABLE IV. Calculated axial and volume compressibilities for the $F_{R(LT)}$, clamped $F_{R(LT)}$, and A_O phases of our PZT95/5(2Nb) ceramic sample. These compressibilities are defined as $(d \ln a/dP)_T$ and $(d \ln V/dP)_T$ and are in units of $10^{-4}/\text{kbar}$.

Phase	Compressibility	T (K)	
		295	200
Normal	κ_a	3.5	3.4
$F_{R(LT)}$ phase	κ_c	6.3	3.9
	κ_V	14	11
	Clamped		
$F_{R(LT)}$ phase	κ_a	2.8	2.3
	κ_c	6.8	6.8
	κ_V	13	11
A_O phase	κ_a	4.8	4.6
	κ_b	1.4	1.0
	κ_c	3.2	2.4
	κ_V	9.4	8.0

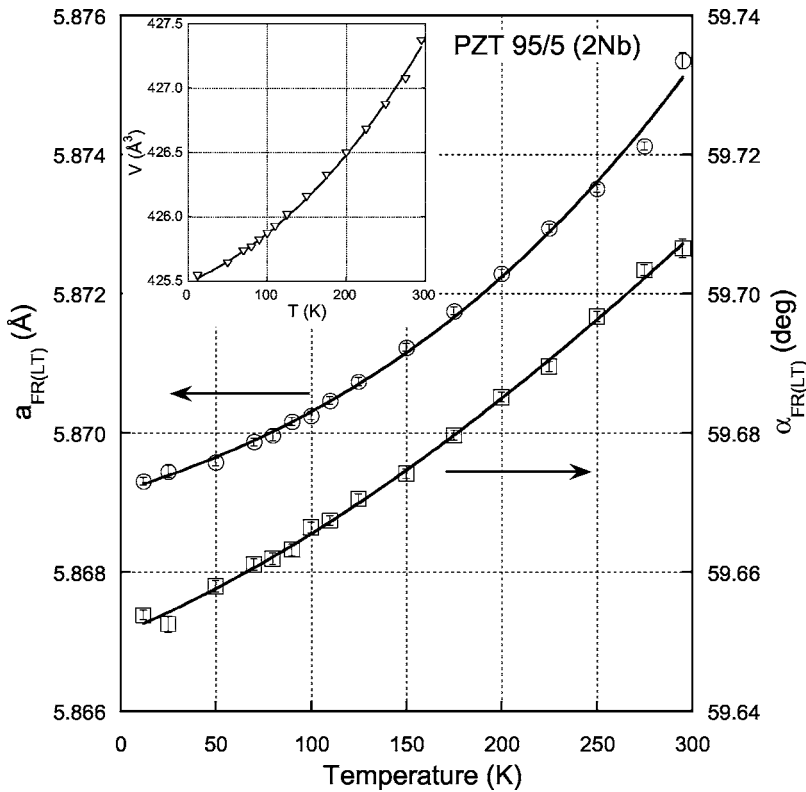


FIG. 14. $F_{R(LT)}$ cell parameters (rhombohedral setting) as a function of temperature (circles for a , squares for α). Inset is the volume as a function of temperature.

threefold polar axis. This rotation is given by the tilt angle $\omega = \tan^{-1}(4e\sqrt{3})$. The P dependences of these parameters are shown in Fig. 12. This approach, with its four parameters, leads to a simpler Fig. 12 than would be the case for an alternate approach, where 14 values of close interatomic separations or bond lengths (not counting corresponding angles) would be involved.

All the parameters at P higher than that of the transition P in Fig. 12 are, expectedly, less accurately determined due to low $F_{R(LT)}$ phase content. Values for the powder sample at room T essentially parallel those of the ceramic with increasing P . The structure parameters given in Fig. 12 show that the atomic positions below the phase transition involve small monotonic changes, i.e., the main structural change is one of the compression of the lattice rather than atomic shifts. These small changes with increasing P involve a slight decrease in s , the Pb structural parameter, and essentially no change in t , the B-site position, or d , the distortion of the oxygen octahedron while the tilt angle ω increases.

At the transition, there appears to be an abrupt change in s which then decreases slightly at higher pressures above the transition. This is more pronounced at 200 than at 295 K. The parameter t appears to increase with increasing P above the transition. There is also an abrupt shift in d at the transition, and it continues to increase with increasing P . The rotation, ω , appears to reverse direction from that below the transition. (Note that as P increases, ω appears to approach zero, the condition for $F_{R(LT)}$ going to $F_{R(HT)}$, suggesting that at higher pressures, should the ever-reducing amount of $F_{R(LT)}$ phase still be present, a phase transition might occur.) Again, it is emphasized that the smaller amount of the minority phase at P results in larger e.s.d. values. Note that on

return to ambient P , because of hysteresis, the $F_{R(LT)}$ phase is still the minority one, and the stress or strain induced by the A_O phase prevents the complete return to the beginning atomic positions. This is evident in Table I, particularly with respect to the oxygen positional parameters and, hence, the tilt angle.

For the majority A_O phase above the phase transition, the structural parameters are given in Table III. The shifts with increasing P tend to be in the same direction for the 200 and 295 K atomic parameters. In most cases, these are only near one or two e.s.d.. They cannot be considered significant using the usual statistical criteria.²¹ The resulting shifts due to T difference are not as pronounced as they were for the $F_{R(LT)}$ phase. The arrows in Fig. 10 indicate the small shifts with P relative to the schematic structure. In the A_O phase, the space group restrictions keep the O1 and O2 oxide ions on the mirror planes at 0 and $\frac{1}{2}$ and the O4 and O5 on the cell edge. Corner sharing allows the octahedra to slightly tip and distort with increasing P .

Recent first-principles calculations have given results on some of these structural details;²² namely, lattice parameters and atomic displacements are in good agreement with those reported above. These calculations also gave relative lattice energies of the various phases.

D. Compressibilities

Figure 13 shows the P dependences of the cell volumes for our ceramic sample at 200 and 295 K, normalized to the cubic perovskite cell by using 1/6 of the hexagonal basis cell for the $F_{R(LT)}$ and 1/8 of the usual orthorhombic cell for the

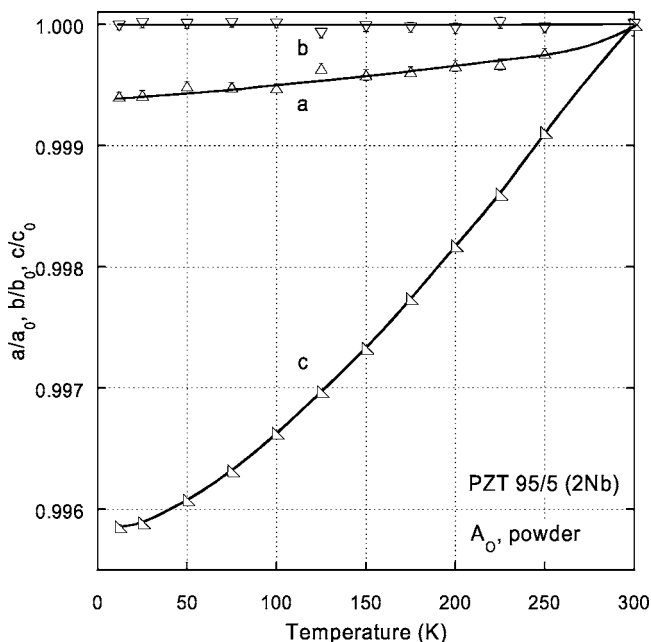


FIG. 15. Temperature dependence for the normalized cell parameters for the A_O phase in the powder sample.

A_O phase in order to put them on a common basis. The discontinuity at the transition and the very slightly lower compressibility above 2 kbar for the $F_{R(LT)}$ phase at 295 K is due to the afore-mentioned clamping by the A_O phase. The filled triangles at 1 bar represent the normalized volumes after releasing the P to ambient for the 295 K run. The volume for the recovered A_O phase agrees with the extrapolation of the volume from values (shown by the dotted lines) above the transition at 2 kbar. The slight displacement of the solid triangle for the $F_{R(LT)}$ phase from the initial value is very likely due to some clamping by the majority A_O phase that did not revert to $F_{R(LT)}$ upon release of the pressure. Values for the powder sample essentially parallel those of the ceramic with a slight shift to a larger normalized cell volume for the A_O phase.

From Figs. 6 and 13 as well as various data runs, the volume and linear compressibilities can be calculated. These are given in Table IV for both the normal and “clamped” $F_{R(LT)}$ and the A_O phases (all values are $\times 10^4/\text{kbar}$). The volume compressibilities are typical for ABO_3 perovskites ($\sim 10^{-3}/\text{kbar}$). These values show that the lattice of the $F_{R(LT)}$ phase is a bit softer than the higher-density A_O phase, as expected, and that both phases are rather anisotropic to compression. The c axis of the $F_{R(LT)}$ phase is significantly softer than the a axis (or along the $\langle 001 \rangle$ than perpendicular to $\langle 001 \rangle$). It is noted that the anisotropic contraction of the A_O cell is accomplished with a minimum in atomic positional displacements.

E. Temperature effects and expansivities

Figure 14 shows the T dependences of the $F_{R(LT)}$ cell parameters and unit cell volume to 12 K at 1 bar for our

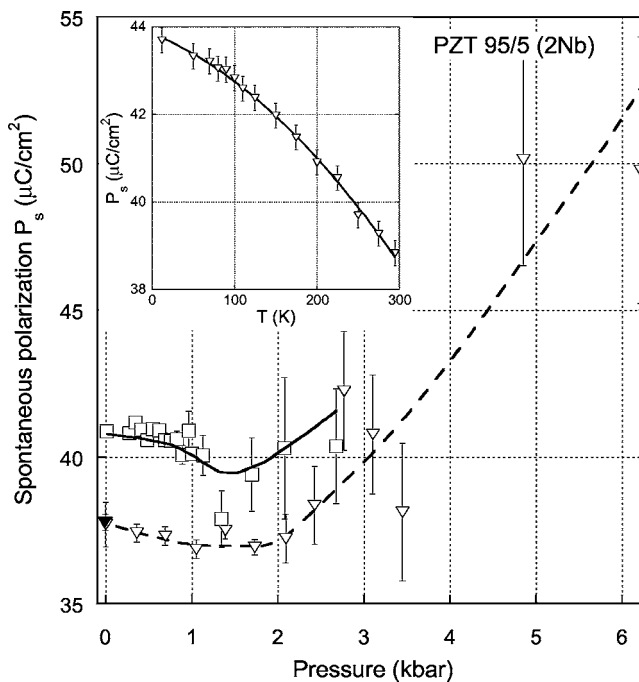


FIG. 16. Spontaneous polarization as a function of pressure (295 K, triangles; 200 K, squares) and temperature at 1 bar (inset) for the $F_{R(LT)}$ phase.

ceramic sample. Values for our powder sample are in excellent agreement and essentially superimpose those given here for the ceramic. It is seen that all these parameters approach 0 K with zero slope as required by the third law of thermodynamics. It is also seen that the thermal expansivities increase with increasing T up to our highest T , 295 K. Ultimately, at higher temperatures, it is expected that there will be a region of constant expansivities, i.e., where the parameters a and V will change linearly with T . At room T , we estimate the expansivities to be $d \ln a/dT = 4.2 \times 10^{-5}/\text{K}$, $d \ln \alpha/dT = 3.8 \times 10^{-6}/\text{K}$, and $d \ln V/dT = 1.8 \times 10^{-5}/\text{K}$.

No phase transition occurred below 300 K at 1 bar in either our powder or ceramic samples. This is consistent with the results of Kojima *et al.*⁶ as well as Yang *et al.*⁷ which indicated a crossing into the A_O phase boundary for a composition near 2.5, but not 3.0, mole % Ti. For undoped or pure PZT95/5, the $F_{R(LT)}$ - A_O phase transition occurs near 233 K.⁷ In the present case at 4.5 mole % Ti, no such transition would be expected for material doped at the 2 at. % Nb level; hence, it was fortunate that our powder sample contained 8 wt % of the A_O phase (Fig. 5). This allows us to obtain the data shown on this phase (Fig. 15). The refinements showed no increase in wt % with decreasing T . This probably suggests that there is a sufficient amount of Nb in this portion of the powder sample and that there might be a small stoichiometric variation of the grains of the powder sample sufficient to cause an initial crossing of the $F_{R(LT)}$ - A_O boundary above room T during synthesis.⁷ Hence a small amount of P is still necessary to increase the A_O phase in our samples.

Temperature has a larger effect than pressure on the atomic positional coordinates as shown by comparing the

TABLE V. Refined structural parameters for $F_{R(LT)}$ phase in ceramic sample of PZT95/5(2Nb) at ambient pressure. Space group $R3c$ (no. 161), with Pb at $6a(0,0,z)$, Zr (Ti) at $6a(0,0,z)$, and O at $18b(x,y,z=1/12)$. Numbers in parentheses are statistical standard deviations of the last significant digit.

	T (K)				
	12	50	100	150	250
a (Å)	5.83856(4)	5.83920(5)	5.84062(5)	5.84228(4)	5.84656(5)
c (Å)	14.4143(2)	14.4145(2)	14.4152(2)	14.4168(2)	14.4200(2)
$z(\text{Pb})$	0.28692(8)	0.28668(9)	0.28630(9)	0.28565(8)	0.28393(9)
$U_{11}(\text{Pb})(\text{Å}^2)$	0.0026(2)	0.0037(3)	0.0061(3)	0.0084(3)	0.0150(4)
$U_{33}(\text{Pb})(\text{Å}^2)$	-0.0003(3)	0.0000(4)	0.0009(4)	0.0033(4)	0.0060(5)
$z(\text{Zr/Ti})$	0.01509(9)	0.01493(10)	0.01475(10)	0.01444(9)	0.01359(11)
$U_{\text{iso}}(\text{Zr/Ti})(\text{Å}^2)$	0.0023(2)	0.0024(3)	0.0026(2)	0.0031(2)	0.0037(2)
$x(\text{O})$	0.1366(2)	0.1367(2)	0.1375(2)	0.1386(2)	0.1412(2)
$y(\text{O})$	0.3493(2)	0.3490(2)	0.3489(2)	0.3487(2)	0.3477(2)
$U_{11}(\text{O})(\text{Å}^2)$	0.0076(4)	0.0079(5)	0.0091(5)	0.0104(4)	0.0146(6)
$U_{22}(\text{O})(\text{Å}^2)$	0.0052(5)	0.0051(5)	0.0055(5)	0.0060(4)	0.0076(5)
$U_{33}(\text{O})(\text{Å}^2)$	0.0054(4)	0.0049(5)	0.0054(4)	0.0065(4)	0.0105(6)
$U_{12}(\text{O})(\text{Å}^2)$	0.0021(5)	0.0017(5)	0.0020(5)	0.0023(5)	0.0029(6)
$U_{13}(\text{O})(\text{Å}^2)$	0.0001(4)	-0.0001(4)	0.0000(4)	-0.0003(4)	-0.0011(5)
$U_{23}(\text{O})(\text{Å}^2)$	-0.0022(3)	-0.0024(4)	-0.0026(3)	-0.0031(3)	-0.0047(4)
R_p (%)	3.49	3.73	3.46	3.20	3.08
R_{wp} (%)	5.25	5.85	5.18	4.64	4.64
χ^2	1.93	1.76	2.00	2.17	1.87

200 and 295 K data in Table I. These structural shifts are seen to continue to lower temperatures in our ambient pressure run to 12 K. Table V shows structural parameters on the ceramic sample at various temperatures. These as well as values from Table I for 200 and 295 K show the atomic positional coordinates change in a monotonic fashion as T is lowered. Such changes on cooling are in the same direction as for P increases.

Values of positional and displacement parameters obtained for the small amount of the A_O phase in the powder sample were of less precision with larger e.s.d.; nevertheless, the positional parameters show similar structural distortion, mainly due to the increasing deviation of the B site– O_2 – B site angle from 180° in the bc plane of the orthorhombic cell (see Fig. 10 top). This makes the b cell parameter almost T independent, and the cell contraction occurs mainly along the c axis (Fig. 15).

F. Spontaneous polarization

From the measured ionic displacement of the ions along $\langle 111 \rangle_p$ we can calculate the spontaneous polarization P_s and its P and T dependences for the $F_{R(LT)}$ phase below the transition P and above it, where $F_{R(LT)}$ is the minority phase, using the equation

$$P_s = \frac{\sum_i (m_i \Delta x_i Z_i) e}{V},$$

where m_i is the crystallographic site multiplicity, Δx_i is the atomic displacement along the polar axis from the position in

the paraelectric phase, $Z_i e$ is the formal charge of the i th ion, and V is the volume of the unit cell.

Results are shown in Fig. 16 for measurements at 200 and 295 K as a function of P . The results reveal small decreases in P_s with increasing P at both temperatures in the low- P $F_{R(LT)}$ phase reflecting the expected decreases in ionic displacements; but the effects are rather small because of the relatively small (1–2 kbar) P range of the stability of this phase. More interesting, however, are the large increases in P_s for the minority $F_{R(LT)}$ phase in the A_O matrix above the phase transitions (at 1.1 kbar at 200 K and 2.1 kbar at 295 K). These increases result from large anisotropic ionic displacements associated with the aforementioned clamping of $F_{R(LT)}$ grains in the A_O matrix (see Fig. 13).

The decrease in P_s with increasing T at a given P in Fig. 16 is the usual effect in ferroelectrics. The inset in Fig. 16 shows the T dependence of P_s for the ceramic sample at 1 bar over a much larger range. Some features of the results in this inset are worth noting. The calculated value of P_s at room T ($\sim 38.5 \mu\text{C}/\text{cm}^2$) is significantly higher than what is typically measured on ceramic PZT95/5(2Nb) samples (31 – $32 \mu\text{C}/\text{cm}^2$). This undoubtedly is due to the fact that not all the FE domains in the sample become aligned with the electric field on poling as well as the existence of residual porosity in the sample in which the density is close to 92% of theoretical (crystal) density. Second, note that there is quite a large increase in P_s on decreasing T from 295 to 12 K. At 12 K, P_s determined from the measured ionic displacements and the normal ionic charges is $\sim 44 \mu\text{C}/\text{cm}^2$.

IV. CONCLUDING REMARKS

The P -induced $F_{R(LT)}-A_O$ phase transition in PZT95/5(2Nb) has been known for a long time, and much of what we knew about it was based on macroscopic measurements such as dielectric spectroscopy and mechanical properties.¹⁻³ Lacking was knowledge of the details of the ionic displacements accompanying the transformation as well as the P and T dependences of these displacements. The present study has provided a detailed view of these effects and revealed much additional insight into the nature and properties of the transformation. Highlights include the following: (1) Quantification of the degree of incompleteness and irreversibility of the transformation; (2) The discovery of the large anisotropic and unusual strains experienced by the untransformed $F_{R(LT)}$ grains that exist as a minority phase in the high- P A_O phase (specifically, the a and c parameters of the minority $F_{R(LT)}$ phase exhibit discontinuous changes at the transition, a increasing and c decreasing in a first-order-like transition manner); (3) The determination of the spontaneous polarization of the $F_{R(LT)}$ phase and its T and P dependences from the measured ionic displacements; and (4) The large increase with P in the spontaneous polarization of the minority $F_{R(LT)}$ phase above the transition. The structural details also provide a basis for comparison with those from first-principles calculations.²²

The dielectric measurements complemented the neutron diffraction study and yielded a detailed T - P phase diagram for our PZT95/5(2Nb) material. Finally, the combined study suggests a significant influence of the configuration (disk thickness and size) of the sample on the observed boundary for the $F_{R(LT)}-A_O$, but not for the $F_{R(LT)}-F_{R(HT)}$, phase transition, due to the anisotropic cell contractions in the case of the former transition. This is an important feature that we believe is always present when studying the influence of P on ceramic samples consisting of randomly oriented, anisotropic grains.

ACKNOWLEDGMENTS

The authors acknowledge S. Lockwood and R. Moore for powder synthesis and processing and M. Rodriguez for initial x-ray powder diffraction measurements. The work at the Argonne National Laboratory was supported by the U.S. Department of Energy, Office of Science, Contract No. W-31-109-ENG-38. The work at Sandia National Laboratories was supported by the U.S. Department of Energy's National Nuclear Security Administration. Sandia is operated by Sandia Corporation, a Lockheed Martin Company, for the Department of Energy under Contract No. DE-AC04-94AL85000.

¹B. Jaffe, W. R. Cook, Jr., and H. Jaffe, *Piezoelectric Ceramics* (Academic Press, New York, 1971), Chap. 7.

²G. A. Samara, in *High Pressure Science and Technology*, edited by K. D. Timmerhaus and M. S. Barber (Plenum Press, New York, 1979), Vol. 1, p. 177.

³I. Fritz and J. Keck, *J. Phys. Chem. Solids* **39**, 1163 (1978).

⁴B. Noheda, J. A. Gonzalo, and M. Hagen, *J. Phys.: Condens. Matter* **11**, 3959 (1999).

⁵C. Garcia, C. Arago, and J. A. Gonzalo, *Ferroelectrics* **272**, 381 (2002).

⁶S. Kojima, N. Ohta, and X. Dong, *Jpn. J. Appl. Phys., Part 1* **38**, 5674 (1999); 1 wt % Nb means 1 wt % Nb₂O₅ (private communication).

⁷P. Yang, J. A. Voigt, M. A. Rodriguez, R. H. Moore, and G. R. Burns, *Ceram. Eng. Sci. Proc.* **26**, 187 (2005).

⁸J. A. Voigt, D. L. Sipola, B. A. Tuttle, and M. Anderson, U.S. Patent No. 5,908,802 (1 June 1999).

⁹P. Yang, J. A. Voigt, S. Lockwood, M. A. Rodriguez, G. R. Burns, and C. S. Watson, *Ceram. Trans.* **150**, 289 (2004).

¹⁰J. D. Jorgensen, J. Faber, Jr., J. M. Carpenter, R. K. Crawford, J. R. Haumann, R. L. Hittermann, R. Kleb, G. E. Ostrowski, F. J. Rotella, and T. G. Worlton, *J. Appl. Crystallogr.* **22**, 321 (1989).

¹¹A. C. Larson, and R. B. Von Dreele, Los Alamos National Laboratory Rep. No. LAUR 86-748, 1994 (unpublished).

ratory Rep. No. LAUR 86-748, 1994 (unpublished).

¹²B. H. Toby, *J. Appl. Crystallogr.* **34**, 210 (2001).

¹³D. L. Corker, A. M. Glazer, R. W. Whatmore, A. Stallard, F. Fauth, *J. Phys.: Condens. Matter* **10**, 6251 (1998).

¹⁴D. L. Corker, A. M. Glazer, J. Dec, K. Roleder, and R. W. Whatmore, *Acta Crystallogr., Sect. B: Struct. Sci.* **53**, 135 (1997).

¹⁵P. Maistrelli, L. Lutterotti, and P. Scardi, *Mater. Sci. Forum*, **166-169**, 495 (1994).

¹⁶B. A. Tuttle, P. Yang, J. H. Gieske, J. A. Voigt, T. W. Scofield, D. H. Zeuch, and W. R. Olson, *J. Am. Ceram. Soc.* **84**, 1260 (2001).

¹⁷H. P. Klug and L. E. Alexander, *X-Ray Diffraction Procedures*, 2nd ed. (John Wiley & Sons, New York, 1974).

¹⁸A. M. Glazer, *Acta Crystallogr., Sect. B: Struct. Crystallogr. Cryst. Chem.* **28**, 3384 (1972).

¹⁹A. M. Glazer, *Acta Crystallogr., Sect. A: Cryst. Phys., Diffr., Theor. Gen. Crystallogr.* **31**, 756 (1975).

²⁰H. D. Megaw and C. N. W. Darlington, *Acta Crystallogr., Sect. A: Cryst. Phys., Diffr., Theor. Gen. Crystallogr.* **31**, 161 (1975).

²¹W. C. Hamilton, *Statistics in Physical Science* (Ronald Press, New York, 1964), pp. 96-122.

²²K. Leung, E. Cockayne, and A. F. Wright, *Phys. Rev. B* **65**, 214111 (2002); see also K. Leung, *ibid.* **67**, 104108 (2003).